Electrochimica Acta 365 (2021) 137282

Contents lists available at ScienceDirect

Electrochimica Acta

journal homepage: www.elsevier.com/locate/electacta

# Advances in the HCl gas-phase electrolysis employing an oxygen-depolarized cathode

Simon Bechtel[a], Andrew R. Crothers[b], Adam Z. Weber[b], Ulrich Kunz[c], Thomas Turek[c], Tanja Vidaković-Koch[d], Kai Sundmacher[a,e,*]

[a] Department Process Systems Engineering, Max Planck Institute for Dynamics of Complex Technical Systems, Sandtorstr.1, D-39106 Magdeburg, Germany
[b] Energy Conversion Group, Energy Technologies Area, Lawrence Berkeley National Laboratory, 1 Cyclotron Road, Berkeley, CA 94720, USA
[c] Institute of Chemical and Electrochemical Process Engineering, Clausthal University of Technology, Leibnizstrasse 17, D-38678 Clausthal-Zellerfeld, Germany
[d] Electrochemical Energy Conversion Group, Max Planck Institute for Dynamics of Complex Technical Systems, Sandtorstr.1, D-39106 Magdeburg, Germany
[e] Department Process Systems Engineering, Otto-von-Guericke- University Magdeburg, Universitätsplatz 2, D-39106 Magdeburg, Germany

ARTICLE INFO

*Article history:*
Received 11 August 2020
Revised 5 October 2020
Accepted 10 October 2020
Available online 20 October 2020

*Keywords:*
Gas phase electrolysis
Chlorine
Electrochemical process
HCl oxidation
Limiting current

ABSTRACT

The electrolysis of HCl to form $Cl_2$ is an integral part of the production of polycarbonates and polyurethanes. In recent years, the direct gas-phase electrolysis was shown to be significantly more efficient than the current state-of-the-art process based on the oxidation of hydrochloric acid. Still, three phenomena significantly limit the performance and industrial applicability of this process and have so far only been investigated theoretically. Firstly, a limiting behavior in the HCl oxidation reaction was observed, which seems to be of purely kinetic origin. Secondly, also in the full-cell employing an oxygen depolarized cathode, a limiting behavior was detected, which however appears to have a different origin. Lastly, the performance of the oxygen reduction is significantly reduced in comparison to classical $H_2$ PEM fuel cells. The present work utilizes a combined experimental and theoretical approach to confirm that the HCl oxidation is purely reaction limited while the limiting behavior in the full-cell system employing an oxygen depolarized cathode is caused by flooding at low reactor temperatures and, lastly, that the reduced performance of the oxygen reduction reaction is a consequence of significant HCl crossover that can be mitigated by means of increased cathode humidification. These insights are furthermore used to operate the HCl gas phase electrolyzer employing an oxygen depolarized cathode at current densities of more than 5000 A/m$^2$ for the first time, while also substituting the previously employed platinum based cathode catalyst with $Rh_xS_y$, decreasing the impact of HCl crossover and allowing for the lowest so far measured cell potentials over a wide interval of current densities.



## 1. Introduction

In light of climate change and the international goal to limit the average global temperature increase to under 2 K compared to pre-industrial levels, the European Union has set the objective of reducing greenhouse gas emissions to 80 to 95 % below the levels of 1990 [1]. The chemical and petrochemical industry is the third largest industrial greenhouse gas (GHG) emitter and responsible for 19.5 % of the overall European industrial energy consumption. Within the chemical industry, $Cl_2$ is the base chemical, whose production is responsible for not only the highest GHG emissions, more than 80 million tons $CO_2$ equivalents in 2015 [2], but also the highest energy demand with 35 TWh of electrical energy consumed in 2010, which corresponds to 17% of the total electricity consumption of the chemical industry in Europe [1]. Chlorine is widely used for the production of organic solvents, monomers and chemicals for water treatment with a capacity of 66 million tons of $Cl_2$ worldwide in 2014. $Cl_2$ is mainly produced by brine electrolysis [1,3]. One third of all substances produced with the aid of chlorine do not contain $Cl_2$ themselves and use the halogen to facilitate intermediate reactions. 50% of the employed $Cl_2$ is discharged in the form of side products like HCl or chloride salts [4]. Exemplary $Cl_2$-facilitated processes with a growing industrial relevance are the production of methylene diphenyl diisocyanate (MDI), with a process capacity of 4.6 million tons in 2011 and a

* Corresponding author at: Department Process Systems Engineering, Max Planck Institute for Dynamics of Complex Technical Systems, Sandtorstr.1, D-39106 Magdeburg, Germany.
*E-mail address:* Sundmacher@mpi-magdeburg.mpg.de (K. Sundmacher).

https://doi.org/10.1016/j.electacta.2020.137282

growth rate of 5%, and toluene diisocyanate (TDI) production, with a production volume of 3 million tons in 2013 [5–7]. In the production of both isocyanates, phosgene, which is synthesized from chlorine and carbon monoxide, is employed as a reactant. Therefore, for each mole of TDI and MDI, two moles of $Cl_2$ are consumed and four moles of HCl emerge as a byproduct. Since processes that potentially consume HCl, like the production of PVC, are growing at a much slower rate, the market for the HCl byproduct is over-saturated [4,8]. One feasible and sustainable solution to this is the electrochemical oxidation of HCl to $Cl_2$, which is then recycled back into the above-mentioned processes, and hence poses another important source of chlorine.

Currently, the most efficient industrially-employed electrochemical process for the oxidation of HCl to chlorine is the Bayer-UHDENORA process, using hydrochloric acid as feedstock and employing an oxygen depolarized cathode (ODC). Recently, our group proposed a novel process based on the direct electrolysis of gaseous HCl, also employing an ODC that promises a 38% lower exergy demand than the Bayer-UHDENORA variant [9]. The energy demand of this gas phase reactor is also $\sim$ 60 % lower than even the most efficient version of the brine electrolysis process employing an ODC [2,6,10]. Given the significant production volume of MDI and TDI and related chemicals, gas-phase electrolysis of HCl has the potential to contribute to a more green and sustainable chlorine sector of the chemical industry.

However, three phenomena have so far been identified to limit the performance and industrial applicability of the gas-phase reactor [11,12]. First, a limiting behavior was observed in half-cell investigations of the HCl oxidation reaction (HClOR) [11]. Second, a full-cell employing an ODC also exhibited a limiting-current behavior that appears unrelated to the HClOR [12,13]. Third, the ODC exhibits significantly reduced performance compared to in the ones employed in low temperature polymer electrolyte membrane (PEM) $H_2$ fuel cells. For these reason, operation of the gas-phase reactor employing an ODC at 5000 A/m$^2$ has so far not been experimentally achieved, and the measured open-circuit voltages (OCVs) of the oxygen reduction reaction (ORR) within the gas-phase electrolyzer of 680 and 750 mV as well as the high activation overpotential suggest that there is significant room for further reducing the cell potential.

A numerical model presented in our recent publications [11,12] suggests a reaction limitation causes the observed limiting behavior in the HClOR, while in the full-cell reactor employing an ODC, flooding and membrane dehydration were identified as the origin of the limiting behavior. Which one of these mechanisms dominates, strongly depends on the thermal management of the cell, which due to the highly exothermal dissociation reaction of HCl in water as well as the high overpotential, is more complex than in classical $H_2$ fuel cells. Based on these insights, reactor optimization strategies were proposed aimed at allowing for operation at current densities $>$ 5000 A/m$^2$ while maintaining low cell potentials. However, so far, these model-based insights and optimization strategies have not been validated experimentally.

Concerning the reduced performance of the ORR, Kuwertz et al. [13] mentioned crossover of HCl from the anode to the cathode and consequent poisoning of their platinum-based catalyst as a possible reason. There is a wealth of publications investigating the effect of chloride anions [14] and even gaseous HCl [15] in the cathode feed stream on the performance of the ORR in $H_2$ PEM fuel cells. Motupally et al. [16] even investigated HCl crossover for a reactor similar to the HCl gas-phase electrolyzer, however with liquid water being fed into the cathode chamber, by means of measuring the decrease of the pH in the cathode chamber. They proposed that up to 0.1% of the HCl fed into the reactor crosses over to the cathode side. However, it is not yet clear whether mainly the crossover of HCl or $Cl_2$ caused the decrease in the pH. Since liquid water is fed into the cathode chamber of this reactor type, the transport of species through the membrane differs significantly from the gas-phase reactor employing an ODC as proposed by Kuwertz et al. [13], which is the focus of the present work. Due to the significant impact on the performance of the ORR, the extent to which HCl and $Cl_2$ are crossing over under realistic process conditions of the gas-phase electrolysis and the impact of this crossover on the performance of the ORR are important to understand for further reactor optimization.

In our previous publications [11] and [12], the limiting behavior observed in both the previous half-cell investigations of the HClOR [8] and the full-cell investigations employing an ODC [13] was analyzed by means of a numerical reactor model of both electrochemical cells. The present work focuses on an experimental validation and deeper understanding of the limiting behavior and the involved physicochemical mechanisms. Moreover, these insights are utilized to operate the reactor at industrially relevant current densities of $>$ 5000 A/m$^2$, which so far has not been achieved. Lastly, the article investigates the extent and importance of HCl and $Cl_2$ crossover in both a gas-phase reactor and a liquid-phase reactor, resembling the one used in the Bayer UHDENORA process. Based on insights from these crossover investigations, $Rh_xS_y$ is employed for the first time in the HCl gas phase electrolyzer as an alternative cathode catalyst that is less prone to chloride ion poisoning.

The outline of this paper is as follows. First, the experimental setups for investigating the HClOR alone and in combination with an ODC are presented together with the setup for investigating the crossover of HCl and $Cl_2$. Subsequently, a numerical crossover model is introduced to support the experimental examinations. In the second part, the crossover of both species and its impact on the ORR is quantified by a combined experimental and theoretical approach. Subsequently, the reaction limitation of the HClOR is experimentally validated and first considerations about the nature of $Cl\cdot$ surface species are made, supported by further simulations with the numerical reactor model published in [11]. Similarly, previous insights from [12] on the limiting behavior in the full-cell setup employing an ODC are validated and used to operate the reactor at current densities of more than 5000 A/m$^2$ for the first time, while also applying a new cathode catalyst to mitigate the effect of HCl and $Cl_2$ crossover.

## 2. Methods

### 2.1. Working principle of the reactor and experimental setup

For a holistic view of the explored phenomena, three different cells are required: a) the full-cell employing an ODC b) the half-cell for investigating the HClOR, c) the half-cell for analyzing HCl and $Cl_2$ crossover, as shown in Fig. 1a-c.

All experiments were carried out employing a cyclone flow cell, as used by Martínez [8]. The working principle and distinct features of this reactor type are described in detail in [8,17,18]. A main feature is a homogenous concentration boundary layer over wide areas of the MEA [17,18]. This allows for a more direct evaluation of mass-transfer and kinetic effects, since, in comparison to a classical flow-field based cells, 2D and 3D effects are minimized.

An exploded view of the half-cell employed for the crossover and HClOR investigations as well as of the full-cell are depicted in Fig. 2a and b, respectively. The cell potential in the crossover and HClOR experiments is measured against a reversible hydrogen electrode (HydroFlex $H_2$-Reference Electrode by Gaskatel, please see #6 in Fig. 2a.

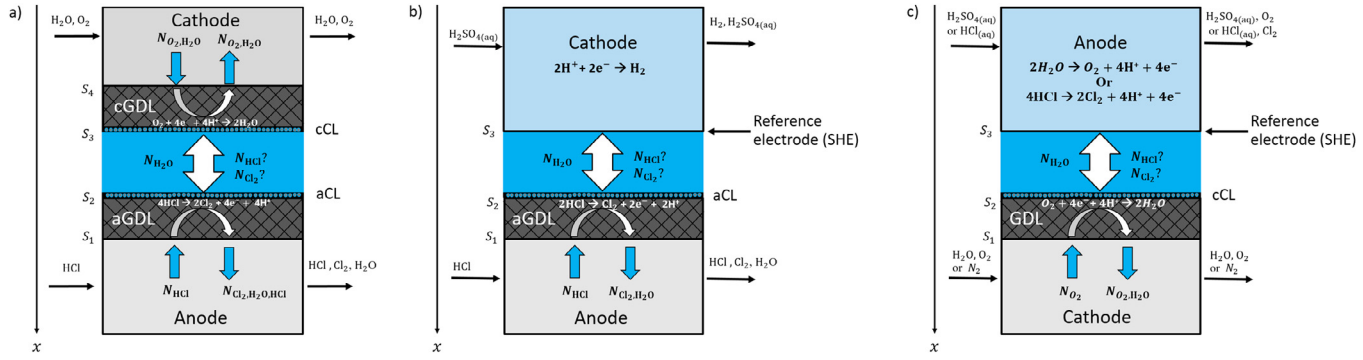


**Fig. 1.** Scheme of the (a) full-cell employing an ODC, (b) the half-cell for investigating the HClOR and (c) the crossover of HCl and $Cl_2$. Adopted from [11],[12].

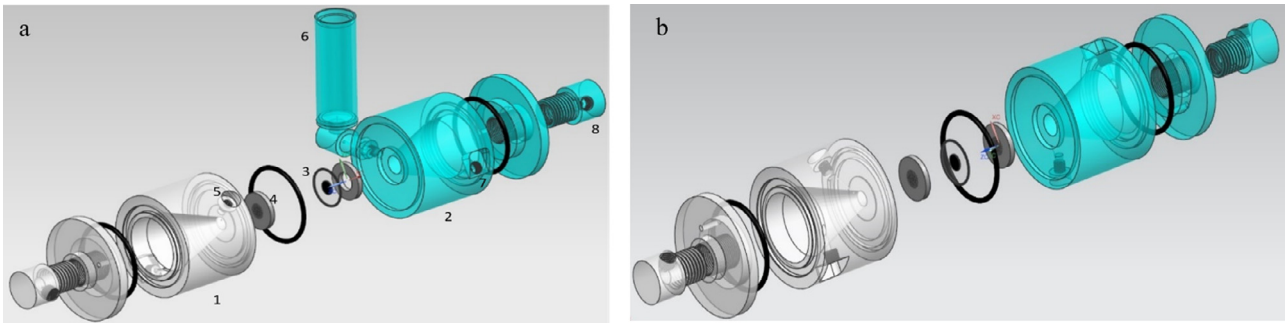


**Fig. 2.** (a) Exploded view of the cyclone flow half-cell consisting of the working electrode compartment (1), the counter electrode compartment (2), the membrane electrode assembly (3), a titanium plate (4) connected to a titanium pin screwed into the orifice (5), which both together work as the current collector, and the reference electrode compartment (6). The reference electrode compartment contains the reversible hydrogen electrode, against which the cell potential is measured in all half-cell experiments. The reactants and electrolyte enter the reactor at the inlets (7) and leave through the outlets (8) that are identical on both sides. (b) Exploded view of the cyclone flow full-cell, equipped with current collectors on both sides instead of a reference electrode compartment. The parts are held together by a titanium frame and six titanium screws fixed with a torque of 17 Nm. (For interpretation of the references to color in this figure, the reader is referred to the web version of this article.)

### 2.2. Membrane-electrode assembly

The membrane-electrode assemblies (MEAs) employed in all half-cell measurements were supplied by HIAT and are based on Nafion115 membranes (Dupont) with a catalyst suspension of Pt/C (60 wt% Pt, by Alfa Aesar) in Nafion applied on one side of the membrane. The final platinum mass loading normalized by cell area is 1 mg/cm$^2$ and the Nafion loading is 0.5 mg/cm$^2$. To facilitate reactant distribution and product removal from the WE, a gas diffusion layer (GDL) (by Quintech) with a thickness of 400 µm is employed. The GDL consists of carbon cloth coated first with a 20 wt% PTFE suspension and subsequently with a mixture of Ketjenblack (Akzo Nobel) and PTFE, generating a microporous layer (MPL), resulting in a total loading of 4.5 mg/cm$^2$ with 20 wt% PTFE. To ensure electrical contact, the MEA by HIAT and the GDL are thermally bonded together at a pressure of 50 bar and a temperature of 398 K for 150 s employing a laboratory press (Polystat 200 T by Servitec). The counter electrode (CE) is a platinum mesh immersed in the electrolyte flowing through the CE compartment of the reactor (see blue colored part in Fig. 2a). Depending on the experiment, the electrolyte is either hydrochloric acid or sulfuric acid (both supra quality by Roth). Since a platinum mesh is employed as a CE, the membrane is only sprayed with catalyst on one side.

In the full-cell measurements, the same MEAs are employed, but additionally, a gas-diffusion electrode (GDE) based on rhodium sulfide ($Rh_xS_y$) serving as the cathode catalyst, is bonded together with the above described MEA, including the anode GDL (aGDL), for 4 minutes at a temperature of 398 K and a pressure of 50 bar. To ensure better contact, the GDE is wetted with a few drops of 5 % Nafion in isopropanol (by Quintech) before the bonding step. The $Rh_xS_y$ GDE was kindly supplied by De Nora and details on its composition are not known. The cell area is 2.27 cm$^2$ in all cases.

To compare the performance of the $Rh_xS_y$ catalyst to the previously employed Pt/C catalyst [13], a second MEA kindly provided by the research group of Prof. Turek at the Technical University of Clausthal was employed. This MEA consists of a Pt/C catalyst (BASF SE) sprayed on a Nafion 117 membrane (Dupont) and two GDLs, all bonded together by the same method as for the $Rh_xS_y$ based MEA. The Nafion 117 membrane was pretreated according to methods adopted in modified form from Ticianelli et al. [19] and Zawodzinski et al. [20]. The platinum loading is 1 mg/cm$^2$ on both the anode and cathode side and the Nafion loading is 2 mg/cm$^2$ on the anode and 0.5 mg/cm$^2$ on the cathode side. The application of the catalyst is done by a wet-spraying process, which is described in detail in [21].

### 2.3. Operation and electrochemical measurements

The gases are supplied via pressurized gas bottles from Linde and are of grade 5 (99.999 % purity) in the case of $O_2$ and $N_2$ and grade 4.5 (99.995 % purity) in the case of HCl. The feed gas flow rates of HCl, $O_2$, and $N_2$ were set to 500 ml/min in all half- and full-cell experiments. The oxygen feed was humidified at 100% relative humidity (RH) with a gas bubbler. All measurements were carried out at atmospheric pressure and room temperature (RT) and neither the feed gases nor the reactor were cooled or heated. To observe temperature changes in the full-cell setup, the temperature of the cathode outlet stream was monitored with Pt 100 thermal sensors and a PCE-T390 thermometer. In the half-cell experiments, no temperature measurements were performed, since

the half-cell can be assumed to be essentially isothermal, due to the strong convective heat dissipation via the electrolyte circulating through the counter electrode chamber [11].

Three different methods; cyclic voltammetry, linear sweep voltammetry, and chronoamperometry, were employed in the investigations involving the half-cell. The full-cell was investigated by means of linear sweep amperometry. Martínez [8] showed that linear sweep voltammetry with a scan rate of 1 mV/s leads to essentially identical polarization curves as steady state measurements. Due to the strong similarity with the experimental reactor of this work, linear sweep voltammetry measurements were recorded with a scan rate of 1 mV/s and linear sweep amperometry measurements with a scan rate of 0.5 mA/s in order to converge towards steady-state behavior. The cyclic voltammograms were performed with a scan rate of 20 mV/s. All experiments were carried out with a ModuLab XM ECS potentiostat (Solartron Analytics) with internal booster allowing for currents up to 2 A.

### 2.4. Numerical model for investigating the crossover of HCl and chlorine

To enhance understanding of HCl and chlorine crossover through the Nafion membrane, a numerical steady-state model was employed. Both species are assumed to absorb in the water constituting the hydrophilic domains of the Nafion membrane. Hence, only the crossover of the aqueous form of $HCl_{(aq)}$ is considered, which, due to the highly exergonic dissociation reaction of HCl in water, appears to be a valid approximation. Similarly, in the case of $Cl_2$, only the transport of dissolved chlorine through the hydrophilic domains of the membrane is considered, while diffusion through the hydrophobic Nafion domain is neglected due to significantly lower diffusion coefficients. At steady state, the divergence of the flux $N_i$ across the membrane (1D, x-direction) is zero for all species $i$ [22].

$$-\frac{\partial N_i}{\partial x} = 0 \tag{1}$$

The water flux across the membrane $N_w$ is defined as

$$N_w = -D_W \frac{\partial c_0}{\partial x} + \frac{\xi}{F} i \tag{2}$$

where $D_w^m$ is the effective diffusion coefficient of water in Nafion considering both hydraulic and diffusive mass transfer [11]. For HCl and $Cl_2$, the flux consists of three terms: convection of the aqueous solution through the membrane, diffusion through the hydrophilic domains, and, for charged $Cl^-$ species, migration [23,24,25].

$$N_i = c_i v - D_i^w \frac{\partial c_i}{\partial x} + \left(\frac{t_i^w}{z_i F}\right) j \tag{3}$$

where $c_i$ is the concentration of species $i$, $v$ is the velocity of the aqueous solution relative to the membrane, $D_i^w$ and $t_i^w$ are the diffusion coefficient and transference number, respectively, of $i$ in the aqueous solution-filled pores, and $z_i$ is the charge number of an ionic species [23].

The two last terms on the right side of Eq. (3) account for diffusion and migration of species relative to the movement of the aqueous solution in the membrane pores, meaning that the aqueous solution is the reference velocity for these terms. The first term accounts for the movement of the aqueous solution relative to the membrane. For well-hydrated membranes considered in this study, the concentration of ions is small compared to the concentration of water in the membrane. As such, the velocity of the aqueous solution through the membrane equals to the velocity of water, $v_w$ [22].

$$v \approx v_w = \frac{N_w}{c_w} \tag{4}$$

Please note that Eq. (3) neglects frictional interactions between the membrane, $Cl^-$, and $Cl_2$ and that the concentrations, velocities, and fluxes have a superficial basis, meaning that quantities are averaged over both the aqueous solution and the hydrophobic Nafion domains of the wet membrane.

The diffusion coefficients $D_i^w$ are challenging to measure and reported values vary by orders of magnitude [26]. In the crossover model, they are calculated by correcting the diffusion coefficient of species $i$ in bulk water $D_i^{0,\infty}$, with $D_{Cl^-}^{0,\infty} = 1.89 \cdot 10^{-9}$ m$^2$/s and $D_{Cl^2}^{0,\infty} = 2.03 \cdot 10^{-9}$ m$^2$/s [27], by the tortuosity of the hydrophilic domains of the membrane $\tau$, where the tortuosity is specified by Archi's law [28].

$$D_i^w = \frac{D_i^{0,\infty}}{\tau} = \frac{D_i^{0,\infty}}{f^{-\chi}} \tag{5}$$

Here, $f$ is the water volume fraction in the membrane and $\chi$ is a scaling coefficient set to 1.33 according to Crothers et al. [29]. The transference number $t_i^m$ in Eq. (3) is related to the diffusion coefficients according to dilute-solution theory [25]

$$t_i^w = \left(\frac{F^2}{RT}\right) \frac{z_i^2 D_i^w c_i}{\kappa} \tag{6}$$

$$f = \frac{V_0 \lambda_M}{V_0 \lambda_M + V_M} \tag{7}$$

where $\lambda_M$ is the water content of the membrane, $V_0$ the molar volume of water, $V_M = \frac{EW}{\rho_M}$ the molar volume of the polymer and $\kappa$ the membrane conductivity calculated as

$$\kappa_M = \kappa_{M,0}(f - 0.042)^{0.88} = 50 e^{\frac{15000}{R}\left(\frac{1}{303.15} - \frac{1}{T}\right)} (f - 0.042)^{0.88} \tag{8}$$

according to [12,30,31]. Solving conservation Eq. (1) with constitutive Eqs. (2) and (3) requires two boundary conditions for each species, adding up to a total of six boundary conditions. Specifying the concentration of species in the membrane at the anode/membrane and cathode/membrane interfaces ($x = 0$ and $x = d_M$ respectively) provides these boundary conditions. The concentration of both species at the cathode/membrane interface is set to zero in all simulations.

As mentioned in the introduction, the crossover of HCl and $Cl_2$ is investigated for the full-cell setup, as proposed by Kuwertz et al. [13], and, in a second scenario, for a liquid-phase reactor resembling the one employed in the Bayer UHDENORA process, where aqueous HCl is fed into the anode chamber instead of gaseous HCl. The concentrations of both species at the interfaces hence vary in both scenarios and are obtained in three steps.

For the full-cell setup, the water content, the partial pressures of $Cl_2$ and HCl in the anode catalyst layer (aCL) and the reactor temperature are extracted from a simulation with the numerical full-cell model introduced in our previous publication [12] as a function of the current density. The reactor feed temperature was set to 333 K, as in [12]. In the second step, these partial pressures are converted into the above-mentioned aqueous interface-concentrations by employing the same vapor/liquid equilibrium relation for HCl-$H_2O$ already used in the full reactor model [11,12] and Henry's law for $Cl_2$ [32].

$$c_{Cl_2}^{\infty} = x_{Cl_2}^{\infty} c_T^{\infty} = \left(9.397\text{x}10^{-4}\ [\text{atm}^{-1}]\right) p_{Cl_2} c_T^{\infty} \tag{9}$$

Here, $p_{Cl_2}$ is extracted from the full-cell model as a function of the current density and given in units of atmospheres and $c_T^{\infty}$ is the total molar concentration of the aqueous solution, which is assumed to be the reciprocal of the molar volume of water (55.6 M). This assumption is valid since the total concentration of the aqueous solution does not change strongly with the concentration of $HCl_{(aq)}$

**Table 1**
Parameters for the numerical simulation of HCl and $Cl_2$ crossover.

| Parameter | Full-cell setup | Liquid phase reactor |
|---|---|---|
| $c^{\infty}_{Cl^-}$ | current density dependent | 2 mol/l |
| $c^{\infty}_{Cl_2}$ | Current density dependent | $1.88{\cdot}10^{-3}c^{\infty}_{T}$ |
| $c^{\infty}_{T}$ | 55.6 mol/l | 55.6 mol/l |
| $K_{M,Cl_2}$ | $f$ | $f$ |
| $K_{M,Cl^-}$ | $0.6363f$ | $0.6363f$ |
| $D^{0,\infty}_{Cl^-}$ | $2.03{\cdot}10^{-9}$ m²/s | $2.03{\cdot}10^{-9}$ m²/s |
| $D^{0,\infty}_{Cl_2}$ | $1.89{\cdot}10^{-9}$ m²/s | $1.89{\cdot}10^{-9}$ m²/s |
| $\chi$ | 1.33 | 1.33 |
| $T$ | 333.15 | 293.15 |
| $d_M$ | 178 µm | 178 µm |

under the investigated conditions [33] and because the concentration of dissolved $Cl_2$ is negligibly small.

In the third step, a partition coefficient, $K_{M,i}$, relates the above introduced concentrations $c_i^{\infty}(p_i)$ to an actual concentration within the membrane $c_i$, considering that possible species-membrane interactions and the presence of the polymer lead to a different concentration of a species in Nafion compared to pure water.

$$c_i = c_i^{\infty}(p_i)K_{M,i} \tag{10}$$

For $Cl_2$, $K_{M,Cl_2} = f$, because this species is not expected to have significant electrostatic or other specific interactions with the membrane and, therefore, it partitions uniformly into the hydrophilic phase of the membrane but not into the hydrophobic polymer regions. Fitting a sorption isotherm from literature for chloride ions in Nafion [34] gives $K_{M,Cl^-} = 0.6363f$. At chloride concentrations relevant for this study (> 0.1 M), the HCl isotherm displays negligible Donnan exclusion, so that this effect is not expected to impede the crossover of $Cl^-$ [34]. The concentrations calculated based on Eq. (10) can then be employed as boundary conditions.

In the second scenario of a liquid phase reactor, the anode chamber is filled with an aqueous solution of hydrochloric acid ($c^{\infty}_{Cl^-}$) of 2 M, which partitions into the membrane according to $K_{M,Cl^-}$. To allow for comparability with the experimental investigations of this work, the temperature was set to 293.15 K. Due to the lack of precise data for $Cl_2$ partial pressures, a value of 1.013 bar is assumed, leading to $c^{\infty}_{Cl_2} = 1.88 \cdot 10^{-3} c^{\infty}_{T}$ [32]. As in the full-cell scenario, the concentration of $Cl^-$ ions and $Cl_2$ in the cathode compartment is set to zero. The membrane water content at the anode membrane interface is set to 17, due to the presence of hydrochloric acid [11]. The cathode is assumed to be at 90% RH, where the membrane has a water content of 10 [35].

Eqs. (1), (2), and (6) were solved simultaneously using the finite element software COMSOL 5.4 with the MUMPS numerical solver. The relative tolerance was set to $1{\cdot}10^{-10}$ and 100 mesh elements were employed. A summary of the relevant model parameters is listed in Table 1.

## 3. Results and discussion

### 3.1. Investigations of the HCl and chlorine crossover in the liquid phase reactor

First, the half-cell setup resembling the Bayer UHDENORA liquid-phase reactor (please see Fig. 1c) is employed to determine to what extend the presence of hydrochloric acid in the anode chamber of the reactor influences the surface properties and the ORR activity of the platinum catalyst in the cathode department. Various literature studies showed that cyclic voltammograms of a platinum electrode immersed in an electrolyte (e.g. sulfuric acid) changes in the presence of chloride anions in three distinct ways.

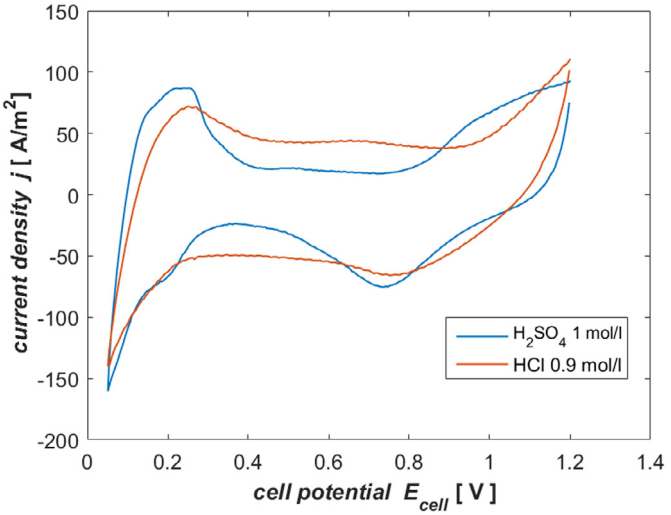


**Fig. 3.** Cyclic voltammograms of the Pt/C WE with sulfuric and hydrochloric acid circulating through the CE chamber referenced versus RHE. Each time, 10 cycles were recorded until essentially no changes in the cyclic voltammograms with increasing number of cycles is observed. The scan rate was 20 mV/s and no ohmic correction was performed.

First, the platinum oxide formation is delayed to higher potentials as a consequence of surface passivation with chloride anions [36,37,38], while oxide formation at higher potentials of more than 1.1 V vs RHE remains mostly unaffected [36]. Second, the corresponding reduction peak declines with increasing chloride concentration [36,37,38]. Last, at ca 0.7 V, an additional peak is observed in the presence of chloride anions that Hudak et al. [36] and Priyantha and Malavipathirana [39] attribute to the reduction of a platinum chloride complex, which might be formed during the oxidative scan.

Fig. 3 shows the cyclic voltammograms measured under $N_2$ atmosphere, when 1 M $H_2SO_4$ or 0.9 M HCl was fed into counter electrode chamber of the half-cell setup. If significant crossover of chloride ions from the CE chamber to the working electrode (WE) does occur, then the two cyclic voltammograms depicted in Fig. 3 should exhibit the above mentioned differences caused by the presence of chloride species.

As expected, the platinum-oxide formation is delayed upon switching from sulfuric to hydrochloric acid, but remains mostly uninfluenced at potentials greater than 1.1 V as in the work of Hudak et al. [36]. Consequently, the reduction peak is also diminished. Whether there is an additional peak caused by the reduction of a platinum chloride complex cannot be determined due to the dominant platinum-oxide reduction peak in the same potential range. While a detailed discussion of these cyclic voltammograms and their implications on the state of the platinum catalyst surface is out of the scope of the present work, the occurrence of the expected phenomena upon changing the electrolyte in the CE chamber to hydrochloric acid implies that indeed HCl or $Cl_2$ are crossing over to an extent that markedly impacts the surface properties of the WE. Please note that this measurement does not allow for a clear differentiation between $HCl_{(aq)}$ and $Cl_2$ crossover, since $Cl_2$ emerges at the CE upon switching from sulfuric to hydrochloric acid and is hence present in the electrolyte.

In an attempt to further understand the influence of this crossover on the ORR, $O_2$ is fed into the WE chamber of the half-cell setup instead of $N_2$ in and a chronoamperometry measurement is carried out starting with 1 M sulfuric acid in the anode chamber at a potential of 0.6 V vs RHE. After 600 s, the sulfuric acid is substituted by 7 M hydrochloric acid without stopping the measurement. The experimental data is depicted in Fig. 4.

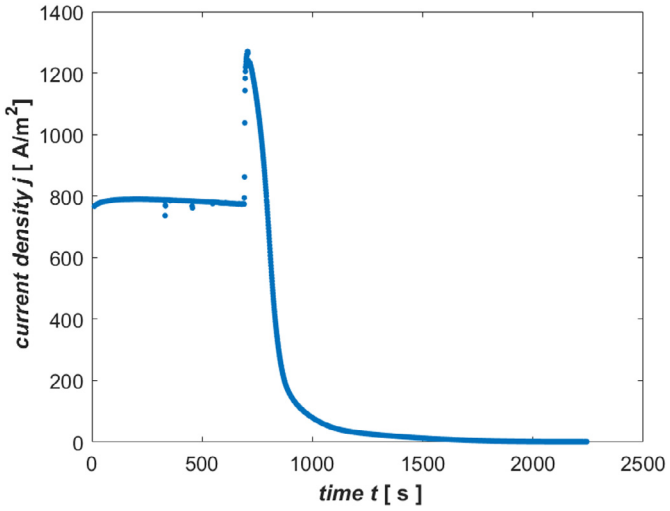


**Fig. 4.** Chronoamperometry at 0.6 V vs RHE with the sulfuric acid stream flowing through the CE chamber being exchanged with hydrochloric acid after 600 s. No ohmic correction was performed.

In the first 600 s, the current density is mostly constant at ca 800 A/m$^2$. The low current density is a consequence of the significant ohmic resistance of the electrolyte and membrane in-between the WE and RE. Upon switching the 1 M sulfuric acid with the more concentrated hydrochloric acid, the current density sharply increases due to the reduced ohmic resistance of the electrolyte. However, shortly after this spike, the current density continuously declines until it reaches a value of essentially 0 A/m$^2$ after 1500 s. As explained in the following, this decay is at least partly caused by chloride ion poisoning.

One contribution to this decay is certainly the negative impact of the 7 M hydrochloric acid on the proton conductivity of the membrane compared to less concentrated sulfuric acid. The ionic conductivity of a Nafion 117 membrane in contact with 1 M $H_2SO_4$ is 0.088 S/cm [40], compared to 0.018 S/cm in the case of 7 M HCl [26], so that switching to a 7 M HCl solution results in a ca. 5 times lower ionic conductivity of the membrane. On the other side, the ionic conductivity of the electrolyte in-between the membrane and the reference electrode is increasing, compensating the above mentioned increase in the total ohmic resistance of the cell. Nonetheless, changes in the ohmic resistance do not account for the full extent of the current-density decay since the ohmic contribution to the overpotential diminishes with lower current densities and hence does not explain the drop to essentially zero current.

Second, the significant differences in the proton activity between the WE and reference electrode reduces the ORR overpotential and hence the current density. The decrease in the ORR-overpotential due to switching from 1 M sulfuric acid to 7 M HCl, approximately $\frac{RT}{F}\ln(\frac{a_{HCl}}{a_{H_2SO_4}})$, should not exceed 0.1 V. Since the OCV of the ORR on Pt/C is known to be at least 0.9 V in the absence of catalyst poisoning species [41], this Nernstian correction does not explain the drop to essentially zero current either. Hence, the significant current density decay must partly be caused by chloride ion poisoning of the platinum based WE. The time scale of the above experiment also shows that the crossover and subsequent catalyst poisoning occurs within a few minutes of operation. Interestingly, Kuwertz et al. [21] measured an OCV of the ORR half-cell reaction of 0.6 to 0.7 V vs RHE in the presence of gaseous HCl in the anode chamber. This is in good agreement with the observed decay of the current density to 0 A/m$^2$ at a potential of 0.6 V.

These experiments show the significant impact of chloride-ion poisoning on the platinum cathode catalyst as a consequence of crossover in the above discussed half-cell experiments. Since furthermore platinum exhibits a lack of stability in the chemically aggressive environment of the HCl electrolysis, especially under open-circuit conditions [42], investigating alternative catalyst materials that are stable and less prone to chloride ion poisoning, is of great importance for the industrial applicability of the process.

To allow for a more quantitative evaluation and a differentiation between the fluxes of HCl and $Cl_2$ through the membrane in the liquid-phase reactor, both fluxes were estimated using the numerical crossover model and are depicted in Fig. 5a for $Cl^-$ and Fig. 5b for $Cl_2$ as a function of the current density. Furthermore, both figures include the contributions of diffusion, convection, and migration to the overall flux.

Fig. 5a and b show a combined crossover of $10^{-3}$ mol/m$^2$/s HCl and $Cl_2$ to the WE chamber. Given the fact that $Cl_2$ is reduced at the cathode and that most of the crossed over species would hence accumulate in the cCL due to the absence of an electrolyte in the WE chamber, and since Schmidt et al. [14] showed that chloride-ion concentrations of $10^{-4}$ M reduce the ORR activity of a carbon supported platinum catalyst by an order of magnitude, such a flux would lead to significant poisoning effects within seconds (at steady state). This once more supports the hypothesis of a crossover related performance decay, at least in the liquid-phase reactor setup.

Moreover, the flux of chloride ions clearly dominates over the flux of $Cl_2$ through the membrane over the whole current-density range. This is mostly due to the fact that while the diffusion coefficient of $Cl_2$ in Nafion is slightly higher than the one of HCl, the concentration of chloride anions in the CE chamber significantly exceeds that of $Cl_2$. The higher HCl concentration leads to an overall increased diffusive and convective flux. The concentration of $Cl_2$ in the CE chamber is set to the upper limit of full saturation of the liquid phase in the simulation, corresponding to a chlorine partial pressure of 1 bar. This estimation was made due to a lack of experimental data and to provide a liberal estimate of $Cl_2$ crossover. Despite this high estimate of $Cl_2$ crossover, chloride anion flux dominates over the $Cl_2$ flux. Hence, the $Cl_2$ flux through the membrane is even smaller than here depicted and can be neglected in the investigated current-density interval.

Another interesting insight is that the flux of chloride species decreases with higher current densities while the $Cl_2$ flux increases. The reason for this becomes clear when looking at the contributions of diffusion, convection, and migration to the overall flux.

As a consequence of the potential gradient in the solution between both electrodes, chloride ions, due to their negative charge, migrate to the anode. According to Ohm's law, this potential gradient is proportional to the current density. For this reason, the migration flux of chloride species depicted in Fig. 5a becomes increasingly negative with higher current densities leading to the discussed decline in the overall flux. In contrast, $Cl_2$ does not migrate due to the electric field because it is not charged.

The second component of the overall flux, convection, increases with current density and becomes the most dominant of all three flux components for both species at intermediate to high current densities (>1000 – 3000 A/m$^2$). It consists of an osmotic component, caused by a water activity gradient across the membrane due to the presence of an aqueous solution in the CE compartment, and an electroosmotic part due to the electroosmotic transport of protons. Consequently, the electroosmotic flux increases linearly with current density. The osmotic flux remains fairly constant over the whole current-density interval because the water content of the membrane is set as a current-density-independent boundary condition on both sides. The slight observable decrease in the osmotic

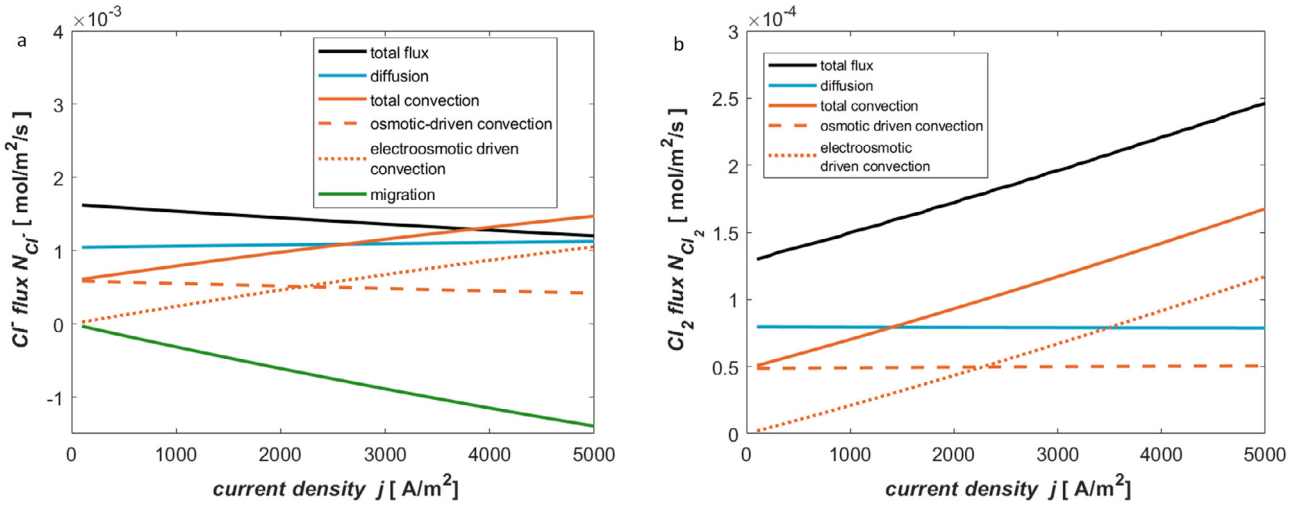


**Fig. 5.** Contributions of diffusion, osmotic-driven convection, electroosmotic-driven convection and migration to the overall flux of (a) $Cl^-$ and (b) $Cl_2$ through the membrane in the liquid phase reactor as a function of the current density.

flux with current density originates in the electroosmotic transport flattening the water concentration gradient in parts of the membrane close to the CE side. Similarly, the boundary conditions for chloride anions and $Cl_2$ also lead to an almost constant diffusive flux across the membrane.

These fixed boundary conditions are an approximation made in the liquid-phase-reactor scenario due to a lack of experimental data on the concentration changes as a function of the current density. One could either experimentally or through a numerical model of the overall liquid-phase reactor determine the boundary conditions as a function of the current density, as done for the gas-phase reactor. However, such studies exceed the scope of the present work.

It can be concluded at this point that the crossover of $Cl^-$ and $Cl_2$ as well as its effect on the ORR is now experimentally and theoretically confirmed for the investigated half-cell resembling the Bayer UHDENORA liquid-phase reactor. Since the concentration of hydrochloric acid in the anode chamber was set to 2 M in the simulation, the crossover of $Cl^-$ anions will be higher in the liquid-phase reactor of the Bayer UHDENORA process where hydrochloric acid at a concentration of ca. 4 M is employed. Furthermore, the numerical model indicates that the crossover of chloride ions dominates over the flux of $Cl_2$ over the whole current-density range. Lastly, operating at higher current densities is not only beneficial in an industrial application due to the decreased cell and stack size, but also because it impedes the crossover of chloride anions significantly.

### *3.2. Investigations of the HCl and chlorine crossover in the gas-phase reactor employing an ODC*

After investigating the $Cl^-$ and $Cl_2$ crossover in the liquid-phase reactor, the following section investigates to what extent these insights can be applied to the gas-phase reactor. Modeling was used to ascertain these effects, where the concentrations of all relevant species at both membrane boundaries and the reactor temperature are taken from the simulation results of the validated numerical full-cell model presented in [12], and are functions of current density.

As Fig. 6a and b show, the flux of chloride ions and, especially, $Cl_2$ through the membrane in the full-cell setup is much lower than in the liquid-phase reactor. The significant reduction in the $Cl_2$ crossover is mainly a result of the lower $Cl_2$ concentration. Moreover, since no liquid water is present in the gas-phase reactor under the investigated conditions, the water content within the membrane is lower compared to the liquid phase reactor, leading to lower partitioning coefficients for $Cl_2$ and $Cl^-$ as a consequence of the reduced membrane water volume fraction $f$. Furthermore, the direction of the convective flux changes, now impeding the transport of both species through the membrane.

On the other side, there is a significantly higher concentration of HCl in the anode of the gas-phase reactor compared to the 2 M solution in the liquid-phase reactor, leading to an increased number of chloride ions in the membrane. Additionally, migration is suppressed in this cell compared to the liquid-phase reactor as a consequence of a lower water content, as can be extracted from Fig. 6a. These effects somewhat offset the reduced crossover resulting from the direction of convection and the low partition coefficient of the gas-phase cell compared to the liquid-phase cell. As a result, there is only a slightly lower chloride-ion flux of $1{\cdot}10^{-4}$ to $8{\cdot}10^{-4}$ mol/m$^2$/s in this cell in comparison to $10^{-3}$ mol/m$^2$/s in the liquid-phase reactor.

The surge in the $Cl_2$ crossover in the gas-phase reactor at higher current densities observable in Fig. 6b is a consequence of the $Cl_2$ production rate in the aCL increasing with the current density (please see Fig. S1 in the supplemental information).

Furthermore, all three flux components (i.e. diffusion, convection, and migration) exhibit significant changes with current density, in comparison to the half-cell investigations. One reason for this is the above-mentioned strong current-density dependence of the membrane water content. Hence, Fig. 7 compares the crossover of $Cl^-$ and $Cl_2$ for three scenarios of different cathode RH. The reference case is the original simulation depicted in Fig. 6a and b, and in both other cases, the water content on the membrane/cathode (M|cCL) interface was increased or decreased by a value of 2 respectively.

Increasing the water content at the membrane-cathode interface, leads to a decrease in the $Cl^-$ and $Cl_2$ flux for all current densities. The reason for this effect is the increase in the osmotic-driven convection with increasing water activity in the cathode resulting in higher water activity gradients across the membrane. Also, the migration component grows with increasing RH. These effects dominate over the increased diffusion flux of both species that comes hand-in-hand with a higher water content leading to the observed reduction in the overall $Cl^-$ and $Cl_2$ flux with increasing RH. Hence, to minimization crossover in an industrial application of the gas-phase electrolysis, it would be beneficial to operate at high cathode RHs.

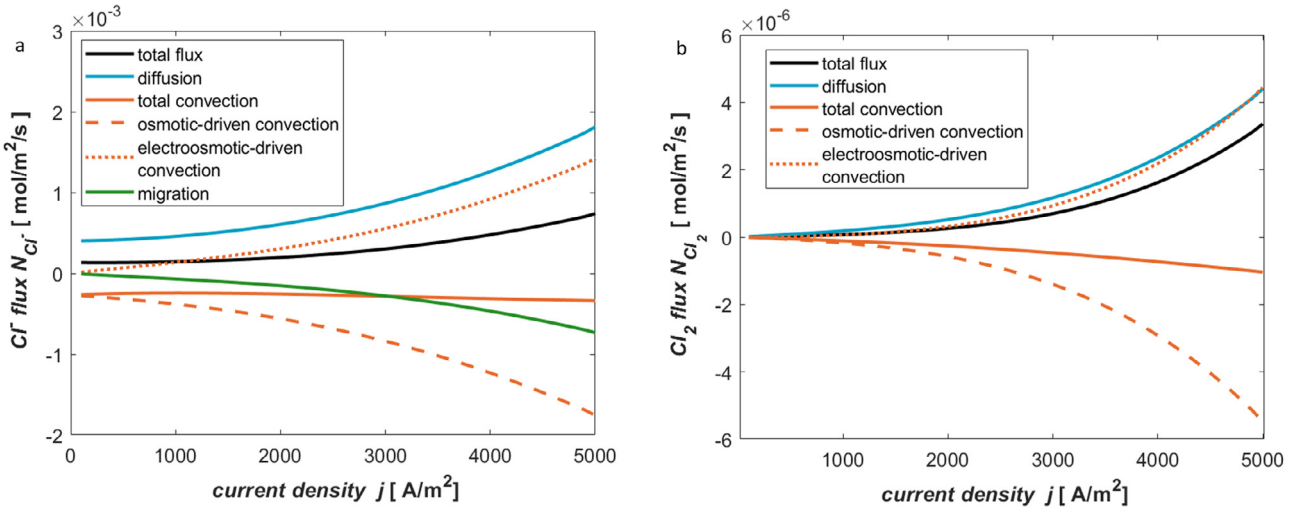


**Fig. 6.** Contributions of diffusion, osmotic-driven convection, electroosmotic-driven convection and migration to the overall flux of (a) $Cl^-$ and (b) $Cl_2$ through the membrane in the gas phase reactor as a function of the current density.

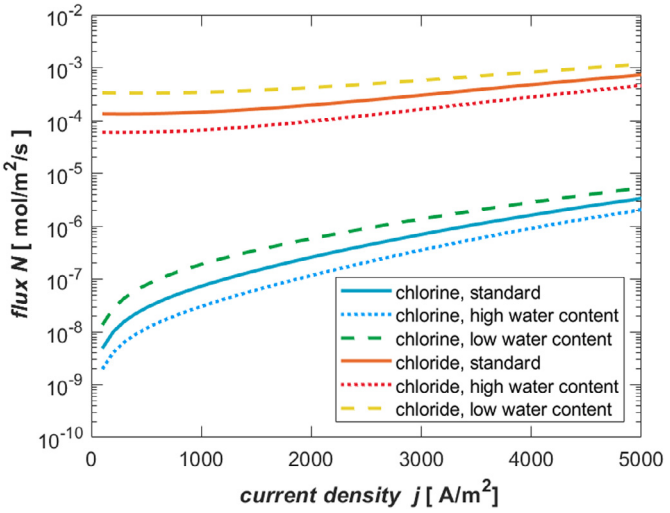


**Fig. 7.** Flux of $Cl^-$ and $Cl_2$ trough the membrane in the gas phase reactor as a function of the current density for three different water contents at the M|cCL interface.

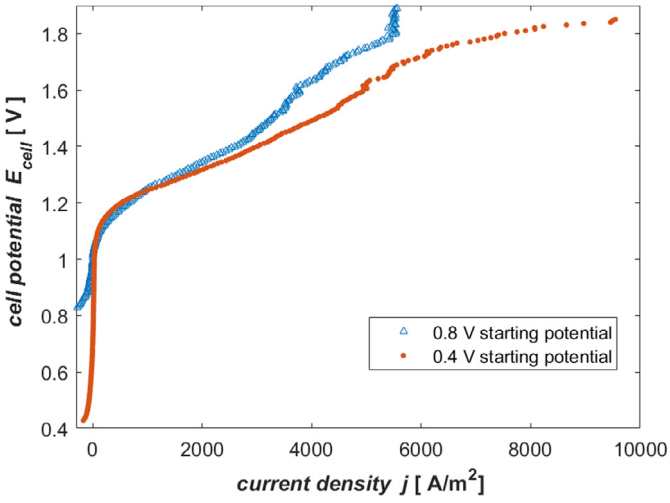


**Fig. 8.** Experimental polarization data for a starting potential of 0.8 V (blue) and 0.4 V (red) measured at RT. The measurements are partly corrected for ohmic resistance online. (For interpretation of the references to color in this figure legend, the reader is referred to the web version of this article.)

### 3.3. Experimental investigations of the HClOR

While earlier publications on the electrochemical oxidation of gaseous HCl attributed the observed limiting behavior to membrane dehydration [43] or mass-transport limitations [8], our recent publication based on the developed numerical reactor model [11] suggests that the limiting behavior is purely kinetic. To be more precise, the chemical Tafel step, in which two adsorbed chloride species recombine forming chlorine, was suggested to be rate determining. Hence, further increasing the cell potential beyond full saturation of the catalyst surface does not accelerate the reaction. In the following, this hypothesis is validated experimentally by investigating the potential history dependence of the limiting behavior in the HClOR.

In Fig. 8, polarization curves of the HClOR measured in the half-cell setup are displayed. Two linear-sweep-voltammetry measurements with a starting potential of 0.4 V and two additional ones with a starting value of 0.8 V were performed. Besides the differences in the starting potential conditions are identical in both measurements. Please note that the observed scattering is likely due to the pulsations of the peristaltic pumps used for the circulation of the electrolyte through the CE compartment of the cell.

The reaction limited current is ca 5500 A/m$^2$ in the 0.8 V case, while no limiting behavior can be observed up to a total current of 2 A, which is the technical limit of the employed potentiostat, in the 0.4 V case. The fact that the limiting current density is potential dependent supports the claim of a reaction limitation instead of a mass-transfer limitation, as explained in the following.

First, there is no difference in the steady-state mass-transfer resistances in between the measurements. It is highly unlikely that transient mass transfer or temperature effects play a significant role either, due to the low scan rate of 1 mV/s in all experiments as well as the convection of sulfuric acid through the cathode chamber and the low conversions leading to almost isothermal conditions. Hence, if mass transfer or membrane dehydration were the cause for the limiting behavior, then the potential history should not impact the limiting current density significantly.

Second, Gilman [44] showed that the adsorption of chloride anions on a Pt electrode immersed in $HClO_4$ containing hydrochloric

acid in low concentrations of $10^{-4}$ M is strongly potential dependent and reversible up to 0.8 V. Above 0.8 V, irreversible formation of PtOH occurs, which competes with the adsorption of chloride anions and vice versa. The author concluded that the surface coverage of chloride species on the catalyst in the potential range of 0.8 to 1.6 V greatly depends on the path taken to reach this potential. Raising the potential from a starting value lower than 0.8 V increases the surface coverage of chloride species also at potentials beyond 0.8 V. Similarly, Arruda et al. [45] showed that already small concentrations of $HCl_{(aq)}$ ($\sim 10^{-3}$ M) severely impaired the formation of Pt-OH at potentials lower than 0.8 V, and upon subsequently increasing the potential to 1.4 V, chloride species remained adsorbed on the catalyst.

In HCl gas-phase electrolysis, chlorine evolution starts at potentials of ca. 1 V, according to the experimental data of Martínez [8]. Contrary to the conditions in the work of Arruda et al. [45] and Gilman [44], adsorbed chloride species recombine at potentials greater than 1 V, forming chlorine and leaving free adsorption sites on which PtCl or PtOH species can again be formed. It is therefore questionable whether the surface coverage still remains a function of the path towards reaching the potential under conditions where chlorine evolution takes place.

Interestingly, Conway and Novak [46] demonstrated that during the oxidation of chloride anions in solution, the formation of platinum surface oxide can be observed upon halting the potential in a potential regime at which chloride oxidation was taking place. Furthermore, the surface oxide charge increased continuously with halting time, even beyond 20 minutes. If this phenomenon is occurring in the HCl gas-phase oxidation as well, it can be expected that the potential history would impact the coverage of chloride anions on the platinum catalyst, even under conditions where chlorine evolution occurs. In that case, if the limiting behavior observed in the experiments of Martínez [8] is indeed a consequence of a reaction limitation in the Tafel step due to the saturation of the catalyst surface with chloride species, the potential history would not only impact the surface coverage but also the reaction-limited current. This is supported by the experimental findings presented in Fig. 8, indicating that the limitation is indeed kinetic.

Furthermore, a shoulder is visible in both polarization curves, indicating a first limitation, which, in the 0.8 V case, is followed by a second, final limitation. Interestingly, Chen and Kucernak [47] observed a similar shoulder and second limitation in their investigations of hydrogen-oxidation reaction (HER) on submicron platinum particles where mass transfer is sufficiently fast to observe kinetic limitations. The authors attribute the shoulder in their polarization data to a kinetic limitation in the Tafel step and the final limiting current density to mass-transfer resistances.

In the following, further possible explanations of this shoulder are discussed. First, a mass-transfer limitation can be ruled out in these measurements. This is supported by our previous model of the HClOR [11] showing that no mass transfer limitations are to be expected until current densities of at least 16000 A/m$^2$. A further interpretation of the observed shoulder could be the onset of the oxygen-evolution reaction (OER) at ca. 1.6 to 1.8 V facilitated by water present in the aCL. For this reason, the HCl feed was subsequently replaced with $N_2$ at the same flow rate and a linear sweep with a scan rate of 5 mV/s was performed. The obtained polarization curve is depicted in Fig. S.3 in the supplemental information and indicates that the OER current is negligibly small even at potentials of up to 2 V compared to the HClOR related current.

Another effect possibly playing a role in the occurrence of the above discussed shoulder could be the HClOR activity of the carbon support, which Martínez [8] proved to be significantly smaller than that of platinum, yet still noticeable at kinetic overpotentials of more than 15 mV. Hence, the acceleration of the HClOR following the shoulder in Fig. 8 could be correlated to the onset of the HCl oxidation on the carbon support.

A further cause that can be ruled out, is the possible involvement of the Heyrovsky step in the reaction kinetics of the HClOR. This reaction cannot exhibit a kinetic limitation as discussed in [11] and [47], but only a mass transport limitation in the diffusion of $Cl^-_{(aq)}$ to the catalyst surface, which was already refuted above.

Another explanation could be the onset of the direct electrochemical formation of hypochlorous acid with a standard potential $E^0 = (1.482 + 0.03pH)$ vs RHE. According to Vos and Koper [48] this reaction is however only competing with chlorine evolution at pH>4 and is hence not likely to play a significant role in the here investigated HClOR due to the highly acidic environment in the aCL.

The most plausible explanation for both the shoulder and the second limitation in the presented data is the presence of at least two Cl· surface species and a reaction limitation in the recombination step of both species (Tafel step), leading to two different limiting-current densities. Chen and Kucernak [47] suggested that there are two different hydrogen species on the catalyst surface, a strongly and a weakly adsorbed one, whose surface coverage exhibit a different potential dependence. Conway and Novak [46] suggested that the brine electrolysis might proceed to a significant extent via Cl· species adsorbed on platinum oxide, presenting a second surface species in addition to PtCl. According to Sabatier's principle, the recombination of Cl· adsorbed on platinum oxide would exhibit a fast rate constant for the Tafel step than the recombination of the more strongly adsorbed PtCl. Hence, the presence of two surface species would result in two limiting-current densities manifesting itself in a shoulder and a subsequent final limiting-current density as observed in the experimental data depicted in Fig. 8.

Which of the two species is responsible for the first and which for the second limiting current density depends not only on the rate constant of the recombination step but also the fraction of active sites that are covered with the respective surface species. This hypothesis is supported by another measurement started at a potential of 1.05 V depicted in Fig. S4 in the supplemental information. For this starting potential, only a minor shoulder is visible in the polarization curve. This might be explained by the fact that, as discussed above, PtCl formation is suppressed by the formation of platinum oxide at potentials higher than 0.8 V. The catalyst surface in this experiment is predominantly covered with oxide species and far less PtCl species compared to the measurements with a lower starting potential. If the chloride oxidation also proceeds via Cl· adsorbed on platinum oxide, as suggested by Conway and Novak [46], the lack of significant amounts of a second adsorbed species (PtCl) would explain the less pronounced shoulder. Similarly, the 0.4 V case exhibits a smaller shoulder than the 0.8 V case, too, which could be again explained by the predominance of one surface species; in this case PtCl.

To further validate this hypothesis, the numerical reactor model presented in [11] was employed to simulate a cell at 333 K with two separate surface species. One species was given a high rate constant but low equilibrium constant of the adsorption/desorption step of chloride species on the catalyst surface $K$, emulating a strongly adsorbed surface species. A second species was given a lower rate constant but increased equilibrium constant, emulating the weakly adsorbed species. The equilibrium constant $K$ is a function of the potential. Due to the difference in the Gibbs free energy of the adsorption/desorption step, the equilibrium constant exhibits a different equilibrium potential. However, this difference can be shifted into the potential-independent prefactor $K_0$ so that the same (over)potential can be employed in the rate expressions

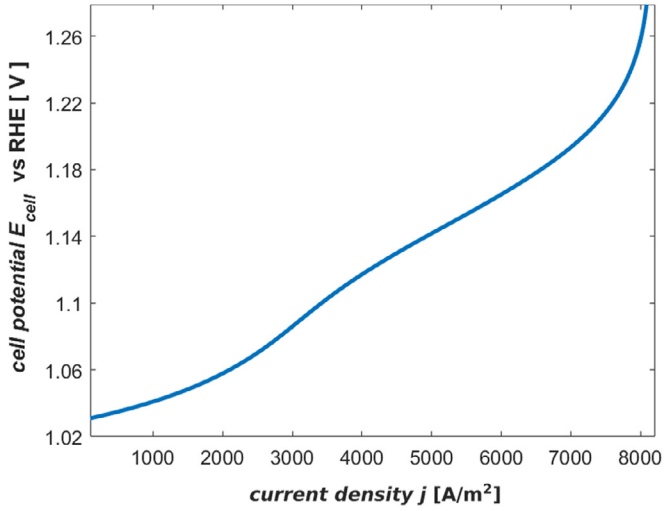


**Fig. 9.** Simulated polarization curve at a temperature of 333 K assuming the presence of two different Cl· surface species.

for both surface species by adjusting $K_0$ accordingly,

$$K = K_0 e^{\frac{\eta_A F}{RT}} \tag{11}$$

The simulation only serves to show the effect of two surface species rather than focusing on their exact adsorption/desorption equilibrium constants. For simplicity, both reactions were modeled in parallel without influencing each other. The simulation results are displayed Fig. 9, exhibiting a shoulder similar to the one observed in the above discussed experimental investigations. The simulation hence provides qualitative justification of the experimental data and supports the hypothesis of a reaction limitation and the presence of two (or more) different surface species.

The fact that the measurements of Martínez [8] do not exhibit such a shoulder indicates that they stopped their experiments at the first limitation. The shoulder and the final limitation should appear if measurements were continued to higher potentials. Indeed, their experimental data [8] demonstrate that the limiting-current density is not fully reached. Alternatively, their high starting potential close to the OCV could be the reason why the catalyst surface is mostly oxidized and hence only small amounts of PtCl were present. This scenario is similar to our measurement at a starting potential of 1.05V, which also barely exhibits a shoulder.

Based on these findings, the limiting behavior observed in these experiments and in the one of Martínez [8] can with great certainty be attributed to a reaction limitation in the Tafel step of the HClOR. If two different surface species are present, this leads to two separate limiting-current densities and hence the formation of a shoulder in the polarization curve. In future investigations, the same methodology could be applied to other catalyst systems that are more resistant to corrosion and dissolution in the aggressive environment characteristic for the HClOR. As such, these systems are more suited for an industrial application of the process. Furthermore, as Fig. 8 shows, reducing the starting potential of the measurement to 0.4 V allows for increased platinum-chloride formation and enables current densities of 10,000 A/m$^2$ with no signs of a limiting current at a temperature of only 298 K. Future investigations should also focus on the stability of this potential history effect over a prolonged course of time. If it is long lasting, it could enable the operation at significantly higher current densities by simply preparing or reforming the catalyst surface with an according potential sweep beforehand or periodically.

### 3.4. Experimental investigations of the full-cell employing an ODC

The model based analysis of earlier polarization curves of Kuwertz et al. [13] indicated that the limiting-current densities observed in both simulation and experiment are mainly a consequence of two opposing mechanisms, namely flooding of the cathode catalyst layer and dehydration of the membrane and anode catalyst layer. Which one of these mechanisms dominates strongly depends on the thermal management of the cell. At ambient conditions and low conversions, as in the experiments of the present work, flooding can be expected. The experiments discussed in the following section aim at validating these insights as well as using them to reach current densities of more than 5000 A/m$^2$, which so far has not been achieved but would be necessary in an industrial application of the process.

Since the model predicts flooding to be at cause for the limiting behavior at low temperatures, a higher HCl flowrate per cell area than in the experiments of Kuwertz et al. [13] was chosen in the experiments of this work. This leads to higher water concentration gradients between anode and cathode due to fast convective removal of water through the anode outlet stream, which increases the water flux through the membrane and hence aids in removing water from the cathode helping to avoid flooding of the cCL.

Furthermore, the reactor is not cooled so that the reactor temperature increases slightly at higher current densities. The increased temperature is also beneficial for delaying flooding of the cathode to higher current densities [12]. As a consequence of the highly insulated cyclone cell, an increase in the reactor temperature appears indeed likely. Due to the small cell area and high reactant flowrates it should however not be significant enough to cause membrane dehydration, as it was known to occur at high reactor temperatures and conversions as well as insufficient cooling [12,49,50]. Furthermore, two different membrane thicknesses (127 and 254 µm) were investigated, as a reduction of the membrane thickness was shown to result in higher limiting current densities [12]. Lastly, since chloride-ion poisoning of the platinum based cathode catalyst was shown to occur, a $Rh_xS_y$ based catalyst was employed. Besides validating the numerical model, the experiments also serve to investigate whether these adjustments in the flowrate, membrane thickness, thermal management and catalyst system indeed lead to the predicted increase in the limiting-current densities to more than 5000 A/m$^2$.

Fig. 10a displays polarization data of two subsequent measurements employing the MEA provided by Clausthal based on Pt/C as a cathode catalyst and a Nafion 117 membrane, while Fig. 10b provides corresponding polarization data employing the $Rh_xS_y$ cathode catalyst and a Nafion 1110 membrane (dry thickness 254 µm). Additionally, Fig. 10b depicts the experimental results from Kuwertz et al. [13], who used thinner Nafion 117 membranes (dry thickness 178 µm), for the same temperature as a benchmark.

Three major conclusions can be drawn from Fig. 10 about the performance of $Rh_xS_y$ as a cathode catalyst, the causes of the observed limiting-current density and, lastly, the impact of these results on the industrial applicability of the HCl gas-phase electrolysis.

The first conclusion to be drawn is that the OCV is closer to the thermodynamic value and the kinetic overpotential is significantly lower when employing the $Rh_xS_y$ catalyst. At a current density of 1000 A/m$^2$, the cell potential is ca −0.64 V for the $Rh_xS_y$ based MEA, -1.15 V for the Pt based MEA and −0.83 V in the measurements of Kuwertz et al. [13]. Moreover, the absolute OCVs and cell potentials are lower than any values recorded by Kuwertz et al. [13] up to a current density of 4500 A/m$^2$, including their measurements at higher temperatures, even though the membrane employed in the present $Rh_xS_y$ experiments is 43 % thicker, leading to increased ohmic losses. This again confirms the above discussed

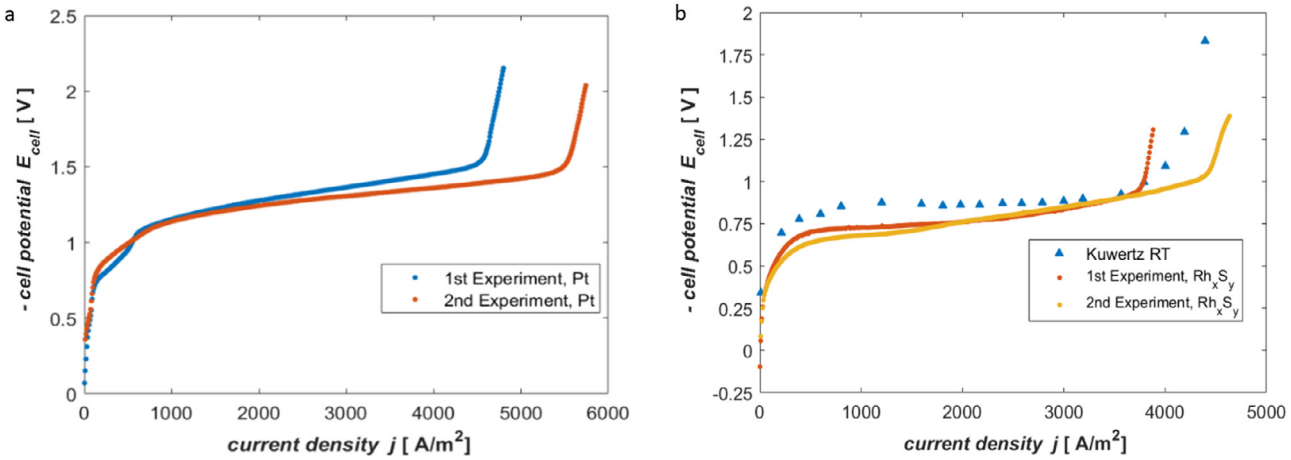


**Fig. 10.** Experimental polarization curves measured at RT employing a) the platinum based cathode catalyst from TU Clausthal on a Nafion 117 membrane and b) the $Rh_xS_y$ based cathode catalyst supplied by De Nora with a Nafion 1110 membrane in comparison to data from Kuwertz et al. [13] (blue). The anode catalyst is platinum and the two experiments are carried out directly after each other in both cases. (For interpretation of the references to color in this figure legend, the reader is referred to the web version of this article.)

hypothesis that chloride-ion poisoning of the cathode catalyst due to HCl and $Cl_2$ crossover has a significant impact on the ORR kinetics on Pt in the gas-phase electrolysis of HCl.

Although the performance of $Rh_xS_y$ compared to Pt-based catalysts for ORR in the presence of hydrochloric acid has already been investigated, for example by Gullá et al. [51], who employed a rotating-disc electrode equipped with both catalysts immersed in hydrochloric acid, this is to our knowledge the first time that $Rh_xS_y$ is being used as a catalyst in the gas-phase electrolysis of HCl employing an ODC. Interestingly, in the work of Gulla et al. [51], the Pt/C based catalyst performed equal to or better than the investigated $Rh_xS_y$ catalysts. The results presented in Fig. 10b however indicate that the $Rh_xS_y$ catalyst outperforms the platinum based one in both the measurements of Kuwertz et al. [13] as well as the present measurements depicted in Fig. 10a. $Rh_xS_y$ has an additional advantage of higher durability. As such, $Rh_xS_y$ is a well-suited system to be employed in an industrial application of HCl gas phase electrolysis. The significantly higher overpotentials in Fig. 10a compared to the data of Kuwertz et al. [13] are likely due to increased uncertainties in the catalyst loading as a consequence of the smaller cell size and the MEA preparation procedure as well as higher anode Nafion loadings.

The second major conclusion concerns the causes of the experimentally observed and simulated limiting behavior and the thermal management of the reactor as discussed in more detail in [12]. The two datasets in Fig. 10a and b correspond to measurements taken directly after each other. Thermal sensors in the oxygen outlet stream showed a temperature increase of 2 K from the start of the first measurement to the end of the second measurement in both cases. Based on the scan rate of 0.5 mA/s and the cell area of 2.27 cm$^2$, each measurement takes approximately 40-50 minutes. As a consequence of the high flowrate per cell area in the present experiment and the geometry of the cyclone flow cell as well as the highly insulating materials it is constructed of, temperatures at the MEA can be expected to be even higher than in the cathode reactor outlet stream. This experimentally observed temperature increase in the second measurements leads to higher limiting-current densities. This fact supports the hypothesis of flooding as cause for the limiting behavior at low feed temperatures and points to the significance of the thermal management as predicted by the numerical model. Furthermore, if flooding is the cause for the experimentally observed limiting behavior, employing thinner membranes should lead to higher current densities [12]. Comparing the limiting current densities of Fig. 10a and b indeed shows an increase in the limiting current densities with reduced membrane thickness. This is confirmed by a last experiment with the same $Rh_xS_y$ catalyst but now employing a Nafion 115 membrane depicted in Fig. 11, displaying again a slight decrease in the limiting current density, further supporting the hypothesis of flooding.

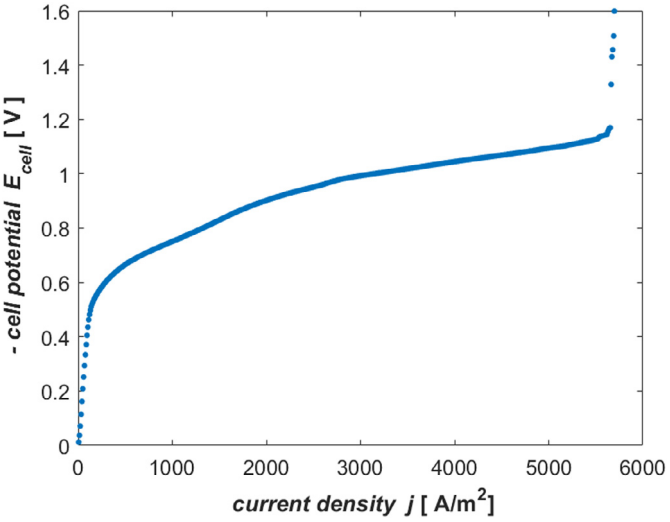


**Fig. 11.** Experimental polarization curves measured at RT employing the $Rh_xS_y$ based cathode catalyst by De Nora and a Nafion 115 membrane.

Interestingly, the slope in the ohmic regime is markedly steeper than in Fig. 10b, even though the membrane is thinner. This might be due to the differences in the membrane water content, although before each measurement, the humidified oxygen stream was fed through the cathode chamber of the reactor for ca. 45 minutes to allow for a comparable membrane water uptake.

The third major conclusion concerns the limiting current density in Fig. 11, which is now ca. 5800 A/m$^2$, exceeding the limiting current density of ca. 4300 A/m$^2$ in the measurements of Kuwertz et al. [13] at the same temperature by 35%. Our results also outperform their higher-temperature measurements. As can be extracted from Fig. 11, the cell potential at 5000 A/m$^2$ is 1.09 V, which is ca. 300 mV lower than the one for the Bayer UHDENORA liquid-phase reactor at the same current density [8,13].

The detailed analysis of the physicochemical phenomena occurring in the gas-phase electrolyzer using the developed numerical model [11,12] and the experimental investigations of the present work allowed for successfully increasing the limiting-current density to an industrially relevant level while maintaining a significantly lower cell potential compared to the Bayer UHDENORA reactor. This result, together with the successful application of a $Rh_xS_y$ based catalyst, is an important step towards the realization of the HCl gas-phase electrolysis on an industrial scale.

While adjustments in the cathode humidification, reactant feed temperatures and other parameters discussed earlier in this work are very likely to further positively affect the performance of the reactor, it should be noted that the cell area in the investigated reactor is comparatively small. In the future, challenges that come with larger cell sizes should hence be tackled by the same combined experimental and theoretical approach, now extending the numerical model to consider 2D and possibly 3D effects complemented by further experimental investigations employing larger reactors.

## 4. Conclusions

In this publication, the origin of the limiting behavior observed in previous experimental investigations of the HClOR and the full-cell employing an ODC, as well as the extent of HCl and $Cl_2$ crossover on the reactor performance was investigated by means of an experimental setup employing a cyclone flow cell, complemented by a numerical crossover model. By investigating the effect of the potential history, the limiting behavior in the HClOR was shown to be a kinetic limitation. We presented the first evidence for the presence of at least two different surface species and discussed the possibility of utilizing the potential history dependence of the limiting-current density for future reactor optimizations. Furthermore, the crossover investigations indicated that significant amounts of HCl permeate through the membrane, impacting the performance of the platinum based ODC and motivating the use of alternative cathode catalyst materials. Interestingly, $Cl_2$ crossover was shown to be negligible under all operating conditions and while operation at higher current densities leads to a reduction in the HCl crossover in a liquid-phase reactor, an increase in the cathode feed humidification appeared to reduce crossover in the gas-phase reactor. Finally, in the case of the full-cell employing an ODC, flooding was confirmed to be the cause of the limiting behavior previously observed. Changes in the reactor operation as well as the catalyst material allowed for achieving current densities of $> 5000$ A/m$^2$ for the first time, while maintaining a significantly lower cell potential compared to the current industrial state-of-the-art reactor in the Bayer UHDENORA process.

## List of Symbols

| | | |
|---|---|---|
| $c_T^\infty$ | Concentration in aqueous solution | $\frac{mol}{l}$ |
| $D_i^{0,\infty}$ | Diffusion coefficient of species $i$ in bulk water | $\frac{m^2}{s}$ |
| $D_i^w$ | Diffusion coefficient of species $i$ in in the aqueous solution-filled pores of the membrane | $\frac{m^2}{s}$ |
| $D_W$ | Diffusion coefficient of water in Nafion | $\frac{m^2}{s}$ |
| $d_M$ | Membrane thickness | m |
| $E_{cell}$ | Cell potential vs RHE | V |
| $EW$ | Equivalent weight membrane | $\frac{kg}{mol}$ |
| $F$ | Faraday constant | $\frac{As}{mol}$ |
| $f$ | Water volume fraction membrane | - |
| $j$ | Current density | $\frac{A}{m^2}$ |
| $K'$ | Equilibrium constant for chloride adsorption/desorption | $\frac{m^3}{mol}$ |
| $K_0$ | Potential independent prefactor | $\frac{m^3}{mol}$ |
| $K_0^*$ | Potential and temperature independent prefactor | $\frac{m^3}{mol}$ |
| $K_{M,i}$ | Partitioning coefficient | - |
| $N_i$ | Flux of species $i$ | $\frac{mol}{m^2 s}$ |
| $p_i$ | Partial pressure of species $i$ | Pa |
| $T$ | Temperature | K |
| $t_i^w$ | Transference number | $\frac{m^2 As}{mol}$ |
| $V_0$ | Molar volume of water | $\frac{m^3}{mol}$ |
| $V_M$ | Molar Volume of polymer | $\frac{m^3}{mol}$ |
| $v_w$ | Velocity water | $\frac{m}{s}$ |
| $\eta$ | Overpotential | V |
| $\kappa_M$ | Ionic conductivity membrane | $\frac{S}{m}$ |
| $\lambda$ | Membrane water content | - |
| $\xi$ | Drag coefficient membrane | - |
| $\rho_M$ | Density of dry membrane | $\frac{kg}{m^3}$ |
| $\chi$ | Scaling coefficient | - |

## Declaration of Competing Interest

The authors declare that they have no known competing financial interests or personal relationships that could have appeared to influence the work reported in this paper.

## Credit authorship contribution statement

**Simon Bechtel:** Conceptualization, Methodology, Software, Validation, Formal analysis, Investigation, Writing - original draft, Writing - review & editing, Visualization. **Andrew R. Crothers:** Methodology, Software, Validation, Formal analysis, Investigation, Writing - review & editing. **Adam Z. Weber:** Writing - review & editing, Supervision. **Ulrich Kunz:** Writing - review & editing, Supervision. **Thomas Turek:** Writing - review & editing, Supervision. **Tanja Vidaković-Koch:** Conceptualization, Writing - review & editing, Supervision. **Kai Sundmacher:** Conceptualization, Writing - review & editing, Supervision.

## Funding

This research did not receive any specific grant from funding agencies in the public, commercial, or not-for-profit sectors. Adam Z. Weber and Andrew R. Crothers would like to acknowledge support from the Department of Energy under contract DE-AC02-05CH11231.

## Acknowledgement and Affiliation

The author Simon Bechtel is affiliated to the International Max Planck Research School (IMPRS) for Advanced Methods in Process and Systems Engineering, Magdeburg, Germany.

## Supplementary materials

Supplementary material associated with this article can be found, in the online version, at doi:10.1016/j.electacta.2020.137282.

## References

[1] A. Boulamanti, J.A. Moya, Energy Efficiency and GHG Emissions: Prospective Scenarios for the Chemical and Petrochemical Industry, Joint Research Centre, European Commission, Petten, 2017 JRC Science for policy report.
[2] A.M. Bazzanella, F. Ausfelder, Low carbon Energy and Feedstock for the European Chemical Industry, Technology study Dechema, Frankfurt: DECHEMA Gesellschaft für Chemische Technik und Biotechnologie e.V., 2017.
[3] S. Rohan, Chlorine Market by Application (EDC/ PVC, C1 & C2 Aromatics, Inorganic Chemicals, Organic Chemicals, Chlorinated Intermediates, Isocyanates, Propylene Oxide, Pulp & Paper, Textiles, Water Treatment, Others), by Region - Trends & Forecasts to 2019, MarketsAndMarkets, Hadapsar, 2015 Market report.
[4] J. Pérez-Ramírez, C. Mondelli, T. Schmidt, O.F.K. Schlüter, A. Wolf, L. Mleczko, T. Dreier, Sustainable chlorine recycling via catalysed HCl oxidation: from fundamentals to implementation, Energy Environ. Sci. 4 (2011) 4786–4799.
[5] M.F. Sonnenschein, Polyurethanes: Science, Technology, Markets, and Trends, 1st ed., Wiley & Sons, Inc., Hoboken, 2015.

[6] ThyssenkruppHydrochloric Acid Electrolysis, ThyssenKrupp Uhde GmbH, Company Brochure, Dortmund, 2012.
[7] Merchant Research, Toluene Diisocyanate (TDI): 2015 World Market Outlook and Forecast up to 2019, Merchant Research and Consulting Ltd, Birmingham, 2015 Market Report.
[8] Martínez, I. G. 2015. Hydrogen chloride electrolysis in a polymer-electrolyte-membrane reactor with oxygen-depolarized cathode. PhD Thesis, Otto-von-Guericke-University Magdeburg.
[9] S. Bechtel, T. Vidaković-Koch, K. Sundmacher, Novel process for the exergetically efficient recycling of chlorine by gas phase electrolysis of hydrogen chloride, Chem. Eng. J. 346 (2018) 535–548.
[10] M. Paidar, V. Fateev, K. Bouzek, Membrane electrolysis—History, current status and perspective, Electrochim. Acta 209 (2016) 737–756.
[11] S. Bechtel, A. Sorrentino, T. Vidaković-Koch, A.Z. Weber, K. Sundmacher, Electrochemical gas phase oxidation of hydrogen chloride to chlorine: model-based analysis of transport and reaction mechanisms, Electrochim. Acta 324 (2019) 134780.
[12] S. Bechtel, T. Vidaković-Koch, A.Z. Weber, K. Sundmacher, Model-based analysis of the limiting mechanisms in the gas-phase oxidation of HCl employing an oxygen depolarized cathode, J. Electrochem. Soc. 167 (2020) 013537.
[13] R. Kuwertz, I.G. Martinez, T. Vidaković-Koch, K. Sundmacher, T. Turek, U. Kunz, Energy-efficient chlorine production by gas-phase HCl electrolysis with oxygen depolarized cathode, Electrochem. Commun. 34 (2013) 320–322.
[14] T.J. Schmidt, U.A. Paulus, H.A. Gasteiger, R.J. Behm, The oxygen reduction reaction on a Pt/carbon fuel cell catalyst in the presence of chloride anions, J. Electroanal. Chem. 508 (2001) 41–47.
[15] O. Baturina, A. Epshteyn, P. Northrup, K. Swider-Lyons, Insights into PEMFC performance degradation from HCl in air, J. Electrochem. Soc. 158 (2011) B1198–B1205.
[16] S. Motupally, A.J. Becker, J.W. Weidner, Water Transport in Polymer Electrolyte Membrane Electrolyzers Used to Recycle Anhydrous HCl: I. Characterization of Diffusion and Electro-osmotic Drag, J. Electrochem. Soc. 149 (2002) D69–D71.
[17] F. Kubannek, U. Krewer, A cyclone flow cell for quantitative analysis of kinetics at porous electrodes by differential electrochemical mass spectrometry, Electrochim. Acta 210 (2016) 862–873.
[18] K. Sundmacher, Cyclone flow cell for the investigation of gas-diffusion electrodes, J. Appl. Electrochem. 29 (1999) 919–926.
[19] E.A. Ticianelli, C.R. Derouin, S. Srinivasan, "Localization of platinum in low catalyst loading electrodes to attain high power densities in SPE fuel cells, J. Electroanal. Chem. Interfacial Electrochem. 251 (1988) 275–295.
[20] T.A. Zawodzinski, C. Derouin, S. Radzinski, R.J. Sherman, V.T. Smith, T.E. Springer, S. Gottesfeld, Water-uptake by and transport through Nafion® 117 membranes, J. Electrochem. Soc. 140 (1993) 1041–1047.
[21] R. Kuwertz, I.G. Martinez, T. Vidakovic-Koch, K. Sundmacher, T. Turek, U. Kunz, Material development and process optimization for gas-phase hydrogen chlroide electrolysis with oxygen depolarized cathode, J. Appl. Electrochem. 46 (2016a) 755–767.
[22] R.B. Bird, W.E. Stewart, E.N. Lightfoot, Transport Phenomena, 2nd ed., Wiley, Hoboken, 2006 Revised.
[23] R.M. Darling, A.Z. Weber, M.C. Tucker, M.L. Perry, The influence of electric field on crossover in redox-flow batteries, J. Electrochem. Soc. 163 (2016) A5014–A5022.
[24] R. Kodým, V. Fíla, D. Šnita, K. Bouzek, Poisson–Nernst–Planck model of multiple ion transport across an ion-selective membrane under conditions close to Chlor-Alkali electrolysis, J. Appl. Electrochem. 46 (2016) 679–694.
[25] J.S. Newman, K.E. Thomas-Alyea, Electrochemical Systems, 3rd ed., Wiley John + Sons, Hoboken, 2004.
[26] T. Vidaković-Koch, I.G. Martinez, R. Kuwertz, U. Kunz, T. Turek, K. Sundmacher, Electrochemical membrane reactors for sustainable chlorine recycling, Membranes 2 (2012) 510–528.
[27] R.C. Weast, CRC Handbook of Chemistry and Physics, 58th ed., CRC Press, Boca Raton, 1978.
[28] F. Dullien, Porous Media Fluid Transport and Pore Structure, 1st ed., Academic Press, Cambridge, 1979.
[29] A.R. Crothers, R.M. Darling, A. Kusoglu, C.J. Radke, A.Z. Weber, "Theory of multicomponent phenomena in cation-exchange membranes: Part II. Transport model and validation.", J. Electrochem. Soc. 167 (2020) 013548.
[30] S. Ochi, O. Kamishima, J. Mizusaki, J. Kawamura, Investigation of proton diffusion in Nafion® 117 membrane by electrical conductivity and NMR, Solid State Ion 180 (2009) 580–584.
[31] A.Z. Weber, R.M. Darling, J. Newman, Modeling Two-Phase Behavior in PEFCs, J. Electrochem. Soc. 51 (2004b) A1715–A1727.
[32] C.L. Young, Solubility Data Series: Sulfur Dioxide, Chlorine, Fluorine and Chlorine Oxides, 12, 1st Edition, Pergamon Press, Oxford, 1983.
[33] S.L. Clegg, A.S. Wexler, Densities and apparent molar volumes of atmospherically important electrolyte solutions. 1. The solutes $H_2SO_4$, $HNO_3$, HCl, $Na_2SO_4$, $NaNO_3$, NaCl,$(NH_4)_2SO_4$, $NH_4NO_3$, and $NH_4Cl$ from 0 to 50°C, J. Phys. Chem. A 115 (2011) 3393–3460.
[34] K.M. Beers, D.T. Hallinan Jr, X. Wang, J.A. Pople, N.P. Balsara, "Counterion condensation in Nafion.", Macromolecules 44 (2011) 8866–8870.
[35] A. Kusoglu, A.Z. Weber, New insights into perfluorinated sulfonic-acid ionomers, Chem. Rev. 117 (2017) 987–1104.
[36] E.M. Hudak, D.W. Kumsa, H.B. Martin, J.T. Mortimer, Electron transfer processes occurring on platinum neural stimulating electrodes: calculated charge-storage capacities are inaccessible during applied stimulation, J. Neural Eng. 14 (2017) 046012.
[37] D.M. Novak, B.E. Conway, Competitive adsorption and state of charge of halide ions in monolayer oxide film growth processes at Pt anodes, J. Chem. Soc. 77 (1981) 2341–2359.
[38] A. Pavlišič, P. Jovanovič, V.S. Šelih, M. Šala, N. Hodnik, S. Hočevar, M. Gaberšček, The influence of chloride impurities on Pt/C fuel cell catalyst corrosion, Chem. Commun. 50 (2014) 3732–3734.
[39] N. Priyantha, S. Malavipathirana, Effect of chloride ions on the electrochemical behavior of platinum surfaces, J. Natn. Sci. Coun. Sri Lanka 24 (1996) 237–246.
[40] S Slade, S.A. Campbell, T.R. Ralph, F.C. Walsh, Ionic Conductivity of an Extruded Nafion 1100 EW Series of Membranes, J. Electrochem. Soc. 149 (2002) A1556–A1564.
[41] J. Zhang, Y. Tang, C. Song, J. Zhang, H. Wang, PEM fuel cell open circuit voltage (OCV) in the temperature range of 23°C to 120°C, J. Power Sources 163 (2006) 532–537.
[42] R. Kuwertz, Energy-efficient chlorine production by gas-phase hydrogen chloride electrolysis with oxygen depolarized cathode PhD Thesis, Technische Universität Clausthal, 2016b.
[43] D.J Eames, J. Newman, Electrochemical conversion of anhydrous HCl to Cl2 using a solid-polymer-electrolyte electrolysis cell, J. Electrochem. Soc. 142 (1995) 3619–3625.
[44] S. Gilman, Studies of anion adsorption on platinum by the multipulse potentiodynamic (M.p.p.) Method. II. Chloride and phosphate desorption and equilibrium surface concentrations at constant potential, J. Phys. Chem. 68 (1964) 2112–2119.
[45] T.M. Arruda, B. Shyam, J.M. Ziegelbauer, S. Mukerjee, D.E. Ramaker, Investigation into the competitive and site-specific nature of anion adsorption on Pt using in situ X-ray absorption spectroscopy, J. Phys. Chem. C 112 (2008) 18087–18097.
[46] B.E. Conway, D.M. Novak, Electrocatalytic effect of the oxide film at Pt anodes on Ci recombination kinetics in chlorine evolution, J. Electroanal. Chem. 99 (1979) 133–156.
[47] S. Chen, A. Kucernak, Electrocatalysis under conditions of high mass transport: investigation of hydrogen oxidation on single submicron Pt particles supported on carbon, J. Phys. Chem. B 37 (2004) 13984–13994.
[48] J.G. Vos, M.T.M. Koper, Measurement of competition between oxygen evolution and chlorine evolution using rotating ring-disk electrode voltammetry, J. Electroanal. Chem. 819 (2018) 260–268.
[49] T.E. Springer, T.A. Zawodzinski, S. Gottesfeld, Polymer electrolyte fuel cell model, J. Electrochem. Soc. 138 (1991) 2334.
[50] V. Stanic, J. Braun, M. Hoberecht, Durability of membrane electrode assemblies (MEAs) in PEM fuel cells operated on pure hydrogen and oxygen, in: Proceedings of the 1st International Energy Conversion Engineering Conference (IECEC), 2003, p. 5965.
[51] A.F. Gullá, L. Gancs, R.J. Allen, S. Mukerjee, Carbon-supported low-loading rhodium sulfide electrocatalysts for oxygen depolarized cathode applications, Appl. Catal. A Gen. 326 (2007) 227–235.